Plant Physiology and Biochemistry 207 (2024) 108354

Contents lists available at ScienceDirect

Plant Physiology and Biochemistry

journal homepage: www.elsevier.com/locate/plaphy

# Mutations in starch biosynthesis genes affect chloroplast development in wheat pericarp

Ermelinda Botticella [a,b,1], Giulio Testone [c,**,1], Valentina Buffagni [a,d], Samuela Palombieri [a], Anna Rita Taddei [e], Domenico Lafiandra [a], Luigi Lucini [d], Donato Giannino [c], Francesco Sestili [a,*]

[a] Department of Agriculture and Forest Science, University of Tuscia, Via S. Camillo de Lellis, 01100 Viterbo, Italy
[b] Institute of Sciences of Food Production (ISPA), National Research Council (CNR), via Provinciale Lecce-Monteroni, 73100 Lecce, Italy
[c] Institute for Biological Systems, National Research Council (CNR), Via Salaria, km 29.300, Monterotondo, 00015, Rome, Italy
[d] Department for Sustainable Food Process, Università Cattolica del Sacro Cuore, Via Emilia Parmense, 84, 29122 Piacenza, Italy
[e] Center of Large Equipments, Section of Electron Microscopy, University of Tuscia, Largo dell'Università, 01100 Viterbo, Italy

ARTICLE INFO

Handling Editor: Shivendra Sahi

*Keywords:*
Wheat
Starch mutants
Seed omics
Side effects
Chloroplast

ABSTRACT

Starch bioengineering in cereals has produced a *plethora* of genotypes with new nutritional and technological functionalities. Modulation of amylose content from 0 to 100% was inversely correlated with starch digestibility and promoted a lower glycemic index in food products. In wheat, starch mutants have been reported to exhibit various side effects, mainly related to the seed phenotype. However, little is known about the impact of altered amylose content and starch structure on plant metabolism. Here, three bread wheat starch mutant lines with extreme phenotypes in starch branching and amylose content were used to study plant responses to starch structural changes. Omics profiling of gene expression and metabolic patterns supported changes, confirmed by ultrastructural analysis in the chloroplast of the immature seeds. In detail, the identification of differentially expressed genes belonging to functional categories related to photosynthesis, chloroplast and thylakoid (e.g. *CURT1*), the alteration in the accumulation of photosynthesis-related compounds, and the chloroplast alterations (aberrant shape, grana stacking alteration, and increased number of plastoglobules) suggested that the modification of starch structure greatly affects starch turnover in the chloroplast, triggering oxidative stress (ROS accumulation) and premature tissue senescence. In conclusion, this study highlighted a correlation between starch structure and chloroplast functionality in the wheat kernel.

## 1. Introduction

Starch fuels plants with carbon and energy for the entire life cycle, and the plasticity of its metabolism can satisfy human needs. The alternation of starch synthesis and degradation (turnover) finely responds to plant-specific energetic demands. Transitory starch is synthesized by chloroplasts during photosynthesis in green tissues, ensuring a steady supply of energy, and it is degraded during the night or in conditions of low light-intensity (MacNeill et al., 2017). Differently, storage starch is the main constituent of seed endosperm and is mobilized to provide energy during germination. Synoptically, starch biosynthesis undergoes two routes that use the adenosine diphospho-glucose (ADP-glucose) as a common substrate and then diverge to polymerize glucose units into amylose (linear α-1,4 glucan) and amylopectin (a highly branched molecule with α-1,4 and α-1,6 glycosidic bonds). Amylose synthesis takes place by the granule-bound starch synthase (GBSS), which exclusively elongates the linear glucan chains, and the GBSSI and GBSSII isoforms respectively act in reserve and transitory starch types (Vrinten and Nakamura, 2000; Tetlow et al., 2004). Amylopectin results from the coordinated enzymatic cascade of starch synthases (SS), starch branching enzymes (SBE), and debranching enzymes (DBE), which, in cereals, have multiple isoforms and activities (James et al., 2003; Botticella et al., 2021). In wheat caryopsis, the concerted action of biosynthetic enzymes determines starch granules made of amylopectin and amylose into a 3:1 ratio (Botticella et al., 2018) which is a crucial parameter in affecting the quality of crops, food,

* Corresponding author.
** Corresponding author.
*E-mail addresses:* giulio.testone@cnr.it (G. Testone), francescosestili@unitus.it (F. Sestili).
[1] Equal contribution.

https://doi.org/10.1016/j.plaphy.2024.108354
Received 24 October 2023; Received in revised form 29 December 2023; Accepted 8 January 2024
Available online 11 January 2024

and industrial applications.

Starch granules are synthesized inside the plastids-chloroplasts or specialized amyloplasts and stored in amyloplasts in the mature kernel (Zhuo et al., 2023; Pfister and Zeeman, 2016). The wheat pericarp is the outer protective tissue covering the mature caryopsis and consists of three layers (epi-, meso- and endocarp). Amyloplasts are found in the mesocarp and provide temporary energy to sustain the whole pericarp growth. At the same time, chloroplasts reside in the endocarp, consisting of two green cell layers (cross- and tube-cells) capable of photosynthesis (Xiong et al., 2013). Seed photosynthesis is thought to exploit $CO_2$ produced from the respiration from surrounding cells to minimize $CO_2$ loss, supply $O_2$ to the endosperm, and manage energy surplus during the grain-filling stage (Kong et al., 2016). In the pericarp, starch accumulation starts a few days after anthesis, peaks at 5 dpa and decreases later on (Yu et al., 2015). Chloroplast degradation and nutrient recycling occur during senescence or because of stress (Choi et al., 2021). Similarly, the accumulation of aberrant starch was observed in maize leaf chloroplasts of *sbe2a* defective lines, characterised by premature senescence and chloroplast altered functions (Yandeau-Nelson et al., 2011). Early senescence events of leaves include changes in chloroplast, such as volume alterations, circular re-shaping, and inner membrane rearrangements (Dominguez and Cejudo, 2021). Moreover, dismantling chloroplasts provoke loss of starch granules, degradation of thylakoids and chlorophylls, increase of plastoglobule number and size, and plastid envelope disruption (Choi et al., 2021; Dominguez and Cejudo, 2021).

Starch metabolism has been widely investigated in cereals (Huang et al., 2021) mostly dealing with the storage type since it is the seed's major compound (60–70%). Consequently, new starch phenotypes have been produced with altered amylose/amylopectin ratio in cereals either for functional studies or food and nonfood industrial applications (Chen et al., 2019). However, the downstream effects of starch modifications in terms of plant adaptation to a varied starch status still need extensive investigation. Additionally, given that some enzymes act in both reserve and transitory starch pathways, their modulation will impact both forms. To date, complex/pleiotropic effects due to starch enzyme mutations in several crops point at starch as a key modulator of carbon metabolism and partitioning, hence influencing the growth of plant organs and seeds (Ragel et al., 2013; Sparla et al., 2014).

Previously, three complete *null* lines of key starch biosynthesis genes (*granule-bound starch synthase I, GBSSI; starch synthase IIa, SSIIa; starch branching enzyme IIa, SBEIIa*) were produced in bread wheat, respectively named Cad-GBSSI*, Cad-SSIIa*, and Cad-SBEIIa* (Botticella et al., 2018). The lines expressed new kernel traits, including the change in amylose/amylopectin ratio, the modification of resistant starch levels, seed hardness and appearance (Botticella et al., 2011, 2018; Sestili et al., 2010a). In this work, morpho-anatomical and omics analyses were conducted on the kernels of these mutants to determine the effects of starch structural changes on grain metabolism. Both differential transcriptomics and metabolite variation profiling highlighted plastid structure and photosynthesis as side targets of altered starch biosynthesis in immature seeds. Chloroplast ultrastructure surveys brought out that the caryopsis endocarp of Cad-SBEIIa* was enriched with chloroplasts with an irregular shape, increased size, and disorganized thylakoid system that was consistent with the altered expression of genes related to thylakoid architecture. Hence, the anomalous branching of amylopectin was proposed to affect the starch turnover equilibria, accumulating irregular granules that activates chloroplast structural alterations and tissue senescence.

## 2. Material and methods

### 2.1. Plant materials

Three different bread wheat *null* mutant lines for *GBSSI*, *SSIIa* and *SBEIIa* genes were previously obtained in *Triticum aestivum* var. Cadenza. The genetic background of these genotypes (Cad-GBSSI*, Cad-SSIIa* and Cad-SBEIIa*) was previously described (Botticella et al., 2011, 2018; Sestili et al., 2010a). The three lines, along with the control Cadenza, were grown in the field at the Experimental Farm "Nello Lupori" (University of Tuscia), located in Viterbo, Italy (lat. 42°26′N, long. 12°04′E, altitude 310 m a.s.l.) in the season 2019–2020. Each genotype was represented by three distinct biological replicates; each was made of a bulk of seeds collected from four spikes harvested at 25 days post anthesis (dpa) (Zadoks growth scale score 83 - Early dough). All seeds sampled were rapidly frozen in liquid nitrogen and stored at −80 °C.

### 2.2. RNA isolation and sequencing

Total RNA was isolated from green seeds harvested at 25 DPA using the SpectrumTM total plant RNA kit (Sigma Aldrich, St. Louis, MO), and quanti-qualitatively assessed by Agilent 2100 Bioanalyzer RNA assay (Agilent Technologies, Santa Clara, CA). Universal Plus mRNA-Seq kit (Tecan Genomics, Redwood City, CA) was used for library preparation following the manufacturer's instructions (library type: fr-secondstrand). The twelve libraries were checked with both Qubit 2.0 Fluorometer (Invitrogen, Carlsbad, CA) and Agilent Bioanalyzer DNA assay, and sequenced in paired-end 150 bp mode on NovaSeq 6000 (Illumina, San Diego, CA). The sequencing provider (IGA Technology Services, Udine, Italy) performed adapter masking of raw fastq with Cutadapt v1.11 (Martin, 2011). All raw RNA-seq data were deposited in the Short Read Archive (SRA) database under the BioProject PRJNA975119.

### 2.3. RNA-seq data analysis

Output reads were checked for quality and filtered to remove ambiguous and low-quality bases respectively using FastQC v0.11.9 (www.bioinformatics.babraham.ac.uk/projects/fastqc/) and Trimmomatic v0.39 (Bolger et al., 2014). High-quality clean reads were aligned to the *T. aestivum* genome sequence of Cadenza ("EIv1.1") by HISAT2 v2.2.1 (Kim et al., 2019). Genome sequence and annotations were recovered from Ensembl Plant Genes (https://plants.ensembl.org), database release 50. StringTie v2.1.5 (Pertea et al., 2015) was executed to assemble transcripts and estimate their abundances in each sample. The transcript expression levels were converted to gene expression levels by tximport v.1.20.0 and DESeq2 package v1.32.0 (Love et al., 2014) was used to perform differential gene expression analyses. Genes were classified as differentially expressed if they differed from the wild-type Cadenza with an adjusted p-value $<0.01$. Principal component analysis was conducted to determine the relatedness of the biological replicates (Fig. S1). Gene ontology (GO) annotations were retrieved from Ensembl Plants and the corresponding Uniprot accessions and used as a reference background for enrichment analysis by using the 'enricher' function implemented in the Clusterprofiler v4.0.5 (Wu et al., 2021). GO terms with corrected p-value $\leq 0.05$ were identified as significantly enriched.

### 2.4. Functional gene annotations

Deduced proteins from the wheat Cadenza "EIv1.1" dataset were used in homology search (BlastP 2.12.0+, e-value $<$ 1e−15) *vs* sequences hosted in NCBI RefSeq (rel. 205) and in Arabidopsis TAIR10 databases. Cadenza candidates involved in starch biosynthesis were searched against homologous sequences previously identified in wheat Chinese Spring background (Gu et al., 2021). The identification of genes encoding chloroplast-related proteins was based on: a) homology to plastid Chinese Spring sequences (Loudya et al., 2021); b) *in-silico* predictions according to the Plant-mSubP tool (http://bioinfo.usu.edu/Plant-mSubP); c) homology to Arabidopsis proteins whose location was inferred by experimental (fluorescence or spectrometry) and/or computational data ("any predictor" in the SUBA5 database, https://

suba.live). Assignment of plastid-related genes was restricted to those genes identified as "plastid" if at least two identification events occurred. Plastid genes were grouped into 18 functional categories according to known functions of respective orthologues in Arabidopsis. Enrichment of differentially expressed genes (DEGs) within functional categories was assessed using the hypergeometric distribution test (phyper function), p-values were adjusted (Benjamini-Hochberg procedure), and the significance level was set at 0.05.

### 2.5. UHPLC/QTOF-MS untargeted metabolomics

Freeze-dried samples were dissolved in extraction buffer (methanol: water 70/30, v/v and 0.1% formic acid) at 20:1: volume-to-weight ratio, and extracted using a blade homogenizer (Polytron PT, Switzerland), centrifuged at 12,000×*g* and filtered through 0.22 μm cellulose filter. Metabolomics analysis was carried out by ultra-high-pressure liquid chromatography (1290 series, Agilent technologies, Santa Clara, CA, USA) coupled to quadrupole-time-of-flight mass spectrometry (G6550 iFunnel, Agilent technologies) via a JetStream dual electrospray ionization source (UHPLC-ESI/QTOF) as previously reported, with slight modifications (Buffagni et al., 2022). Metabolites were separated by reverse phase chromatography under a water-acetonitrile linear gradient elution (6–94% acetonitrile in 33 min) and acquired in full-scan mode (100–1200 m/z), positive polarity and extended dynamic range mode (nominal mass resolution = 30,000 FWHM). Two independent replicates per sample were injected. Quality Controls (QCs) were obtained by pooling all samples and acquired throughout the analysis. QCs underwent the same chromatographic conditions used for samples but acquired in data-dependent MS/MS mode (1 Hz, 50–1200 m/z, 12 precursors per cycle) at different collision energies (10, 20 and 40 eV). Raw data were processed and putatively annotated using Profinder B.07 (Agilent Technologies) and the comprehensive database PlantCyc 9.6 (Hawkins et al., 2021), by the combination of the monoisotopic accurate mass and isotopic pattern (i.e. isotope spacing and ratio) following mass accuracy tolerance of <5 ppm. The annotation process corresponded to level 2 of confidence as set out in the COSMOS metabolomics standards initiative (Salek et al., 2015). Features not present in 75% of replications (n = 6) within at least one treatment were discarded.

### 2.6. Metabolomics data analysis

The metabolomics dataset was elaborated using Mass Profiler Professional 12.6 (Agilent Technologies) following log2 transformation, normalization at the 75th percentile, and baselining against the median abundance of each compound (Ganugi et al., 2022). The relatedness of metabolomic patterns was naively inferred through hierarchical cluster analysis (Euclidean distance, Ward's linkage) based on fold-change (FC) values. Differential compounds were identified by combining ANOVA Tukey HSD analysis ($p < 0.05$; Bonferroni multiple testing correction) and FC analysis (cut-off ≥1.5) and then exported into the Omic Viewer Pathway Tool of PlantCyc (Stanford, CA, USA) software (Caspi et al., 2013) for interpretations and enrichment analysis (Buffagni et al., 2022). In addition, the metabolomics dataset was imported into SIMCA 13 software (Umetrics, Malmo, Sweden) and UV-scaled to perform supervised orthogonal projection to latent structures discriminant analysis (OPLS-DA). OPLS-DA models were cross-validated (CV-ANOVA p = 7.31e-12) and inspected for suspect and strong outliers using 95% and 99% respectively according to Hotelling's T2. After that, model parameters including the goodness-of-fit (R2Y 0.99) and goodness-of-prediction (Q2Y 0.92) were recorded, and model overfitting was excluded by permutation testing (n = 200). Finally, the Variable Importance in Projection (VIP) selection method was used to identify metabolites having the highest discriminant potential (VIP ≥1.2).

### 2.7. Transmission electron microscopy (TEM) and light microscopy (LM)

Samples were fixed overnight at 4 °C with 2.5% (v/v) glutaraldehyde+ 2% (v/v) paraformaldehyde in 0.1 M Phosphate Buffer (PB), pH 7.4. After 3 × 15 min washings at 4 °C in the same buffer, samples were post-fixed with 1% (v/v) osmium tetroxide in 0,1 M PB, pH 7.2 for 1 h at 4 °C. Specimens were washed in distilled water (3 changes for 15 min each at 4 °C) and dehydrated in a graded ethanol series. Samples were then infiltrated with mixtures of LRWhite/ethanol in different percentages, and, at the end of the procedure, they were embedded in LRWhite resin. The polymerization occurred in tightly capped gelatine capsules for 24 h at 50 °C. Ultrathin sections were obtained using a Reichert Ultracut ultramicrotome with a diamond knife, collected on copper grids, stained with uranyl acetate and lead citrate, and observed with a JEOL 1200 EXII electron microscope. Micrographs were captured by the Olympus SIS VELETA CCD camera equipped with iTEM software.

For Light microscopy, semithin sections (1 μm) were collected onto slides, stained by Toluidine Blu and observed at a Zeiss (Axiophot) microscope equipped with a color video camera (Axio Cam MRC) using a computer-assisted image analysis system (AxioVision).

## 3. Results

### 3.1. Transcriptome sequencing and differential expression analysis

The grain transcriptomes of mutant lines were investigated by RNA-seq in order to deepen the characterization of the starch metabolism and to assess putative pleiotropic effects by mining transcriptional divergences among mutants (Cad-GBSSI*, Cad-SSIIa* and Cad-SBEIIa*) *vs* the wild type (Cadenza) plants. Overall, ca. 285.4 million read pairs were generated from sequencing the four transcriptomes (12 paired-end libraries; mean sequencing deep of ca. 47 million reads per sample). After quality assessment and data filtering, ca. 256.7 million high-quality read pairs were recovered, and 82.3–93.3% were successfully aligned to the Cadenza reference genome EIv1.1 (Table S1). PCA explained ca. 82% of the total variance (Fig. S1), clustered the samples according to the respective genotypes, and showed good repeatability among replicates. As compared to the control line, the number of differentially expressed genes was maximal in Cad-SSIIa* (2829), followed by Cad-SBEIIa* (2386) and Cad-GBSSI* (1388). Moreover, the levels of down-regulation generally exceeded that of up-regulation in terms of fold change. Indeed, more than 64% of total DEGs were downregulated in Cad-SBEIIa*, Cad-SSIIa*, and Cad- GBSSI* *vs* control line (Fig. 1A). A proportion ranging from 40% to 74% of DEGs (dark grey bars in Fig. 1B) shared among two or more mutants and the majority of shared DEGs (603) was regulated consistently among all mutant genotypes (Fig. 1A). Furthermore, a fraction ranging from 26.0% to 60% was specifically altered in each mutant (colored bars in Fig. 1B).

### 3.2. Differential expression of genes associated with the starch pathway

Overall, 132 starch biosynthesis genes were identified in the Cadenza genome (Table S2), including 59 genes involved in the generation of ADP glucose (*SUS, INV, AGPase, FK, HK, PGI, PGM*), 30 genes coding related transporters and translocators (*Bt, GPT, SUT*), and 43 genes of amylose and amylopectin synthesis (granule-bound starch synthases, starch branching enzymes, and debranching enzymes). Among them, ca. 30% had undetectable expression levels across the four genotypes and were set apart from further processing (Fig. S2A; Table S2). Differential expression analyses of starch biosynthesis-related gene set revealed that Cad-SBEIIa* had the higher number of DEGs (23 up, 4 down) within, followed by Cad-GBSSI* (8 up, 3 down) and Cad-SSIIa* (4 down), whilst 96 genes were not significantly altered in the three genotypes (Table S2). Most of the DEGs fell in the amylose and amylopectin routes (Fig. S2B), whilst genes coding products acting in the upstream biosynthetic steps did not reveal substantial modifications of expression patterns (except

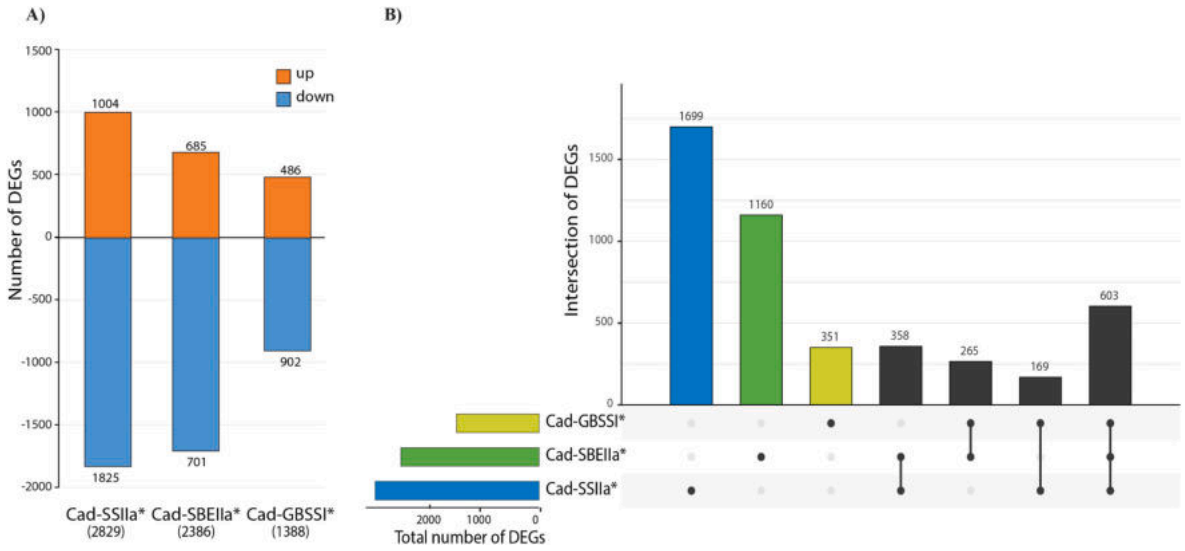


**Fig. 1.** Graphs of differentially expressed genes in starch mutants as compared to wild type lines. (A) Number of up- and down-regulated genes in each mutant. Total number of DEGs per genotype is in parentheses. (B) Number of common and genotype specific DEGs. Colored vertical bars correspond to the number of genotype specific DEGs. Dark grey bars indicate the number of DEGs shared by two or more genotypes. The number of genes in each set is above the bars. In the lower panel, single and connected dots indicate the genotypes (names are on the left panel) sharing each gene set.

for *SUS1-4*, *Bt-1*, and *Bt-3* in Cad-SBEIIa*; *SUS1, SUS5* and *HK* in Cad-SSIIa*; *SUS1, Bt3* in Cad-GBSSI*). Taken together, these data confirmed pleiotropic effects on the transcription of starch key genes and suggested that the plastid environment is likely to be one of the most affected compartments.

### 3.3. Gene ontology (GO) enrichment analyses

GO enrichment analysis was carried out to gain clues on the functional roles of DEGs retrieved from the mutant *vs* wild-type comparisons. The analysis revealed that 54, 51 and 27 terms were enriched of DEGs respectively in Cad-SBEIIa*, Cad-SSIIa* and Cad-GBSSI* (Fig. 2, Tables S3–S4). A high fraction of the enriched classes was common among the mutants, whilst others were genotype-specific. Several shared terms could be ascribed to structure (e.g., chloroplast; chloroplast envelope; chloroplast thylakoid membrane; photosystem I; photosystem II; photosystem II oxygen-evolving complex) and functioning (e.g. photosynthesis; photosynthesis, light harvesting; chlorophyll binding; 2 iron, 2 sulfur cluster binding) of plastids. Moreover, specific terms could be identified for each genome suggesting the occurrence of genotype-specific alterations. Specific terms included 'plastoglobule' and 'sucrose synthase activity' in Cad-SBEIIa*, 'thylakoid', 'sulfate transmembrane transporter activity', 'secondary active sulfate transmembrane transporter activity', and 'sulfate transport' in Cad-SSIIa*, and 'nutrient reservoir activity' in Cad-GBSSI*.

### 3.4. Untargeted metabolomics profiling of mutant lines

Overall, 2943 metabolites were annotated and filtered to 1758 (Table S6) associated to Cad-GBSSI*, Cad-SSIIa*, Cad-SBEIIa* and the wild type (respectively 1745, 1742, 1748 and 1746 compounds). The unsupervised fold-change based hierarchical cluster analysis (HCA) depicted the relationship between the four metabolic signatures and was effective in merging Cad-GBSSI* and Cad-SBEIIa* in the same sub-tree, pointing at similar metabolic signatures and comparable accumulation patterns; differently, Cad-SSIIa* grouped per se (Fig. 3a). The OPLS-DA supervised statistics allowed the separation of the predictive and orthogonal components of variance and all mutant genotypes significantly diverged from the wild type (Fig. 3b). Cad-GBSSI* and Cad-SBEIIa* again grouped into the same score-plot whereas Cad-SSIIa* separated along the first component. Overall, HCA and OPLS-DA concurred to highlight genotype specific metabolic variations that were alike in Cad-GBSSI* and Cad-SBEIIa* lines, and more peculiar in Cad-SS IIa* (Fig. 3a, b). Additionally, the score of variable importance of projection analysis (VIP score >1.2) identified the 118 highest discriminant metabolites (Table S7). They included 4-monogalactosyldiacylglycerols (MGDG), compounds shared in the electron carrier and vitamins biosynthesis (e.g. R-pantoate, phylloquinol, phytyl diphosphate), intermediates of ubiquinol (3-nonaprenyl-4-hydroxybenzoate, *all trans*-decaprenyl-2-methoxy-6-1,4-benzoquinol) and tocopherol pathways (3-(4-hydroxyphenyl)pyruvate, phytil diphosphate). Other compounds belonged to secondary metabolites, mainly terpenoids, and hormones such as auxins (e.g. 3 indole-3-acetate conjugates), brassinosteroids and gibberellins.

In order to bring up metabolites specifically regulated in the mutant lines vs control, Volcano statistics were effective to identify 88 compounds (compound list, LogFC and p-values are in Table S8). The graph of major biochemical changes pinpointed a general negative modulation of primary and secondary metabolites (negative values of Sum logFC in Fig. 4A). However, a fold-change increase (positive values) occurred for fatty acids/lipids and secondary metabolites (Cad-SSIIa*), amines (Cad-SBEIIa*) and cofactors of the porphyrin (Cad-GBSSI*). The number of discriminant compounds was 66 in Cad-SSIIa* (20 up- and 46 down-accumulated), 47 in Cad-SBEIIa* (11 up- and 36 down-accumulated) and 41 in Cad-GBSSI* (13 up- and 28 down-accumulated). Although the mutants shared most compound variations, genotype-specific modulations were identified (Fig. 4B). Briefly, Cad-SSIIa* showed the highest number of unique metabolites (12 up, 17 down), followed by Cad-SBEIIa* (7 up, 6 down) and Cad-GBSSI* (7 up, 2 down). Finally, pathway enrichment analysis showed that significant modulation encompassed several intermediates of amino acid and chlorophyll syntheses, secondary metabolites (such as tocopherols, lignans and quinols) and auxin conjugates (Table S9).

### 3.5. Alteration of the chloroplast structure in immature grains of mutant lines

As the transcriptomic and metabolomic analyses highlight differences among mutant lines and control in the regulation of key genes and metabolites involved in photosynthesis and starch biosynthesis, the

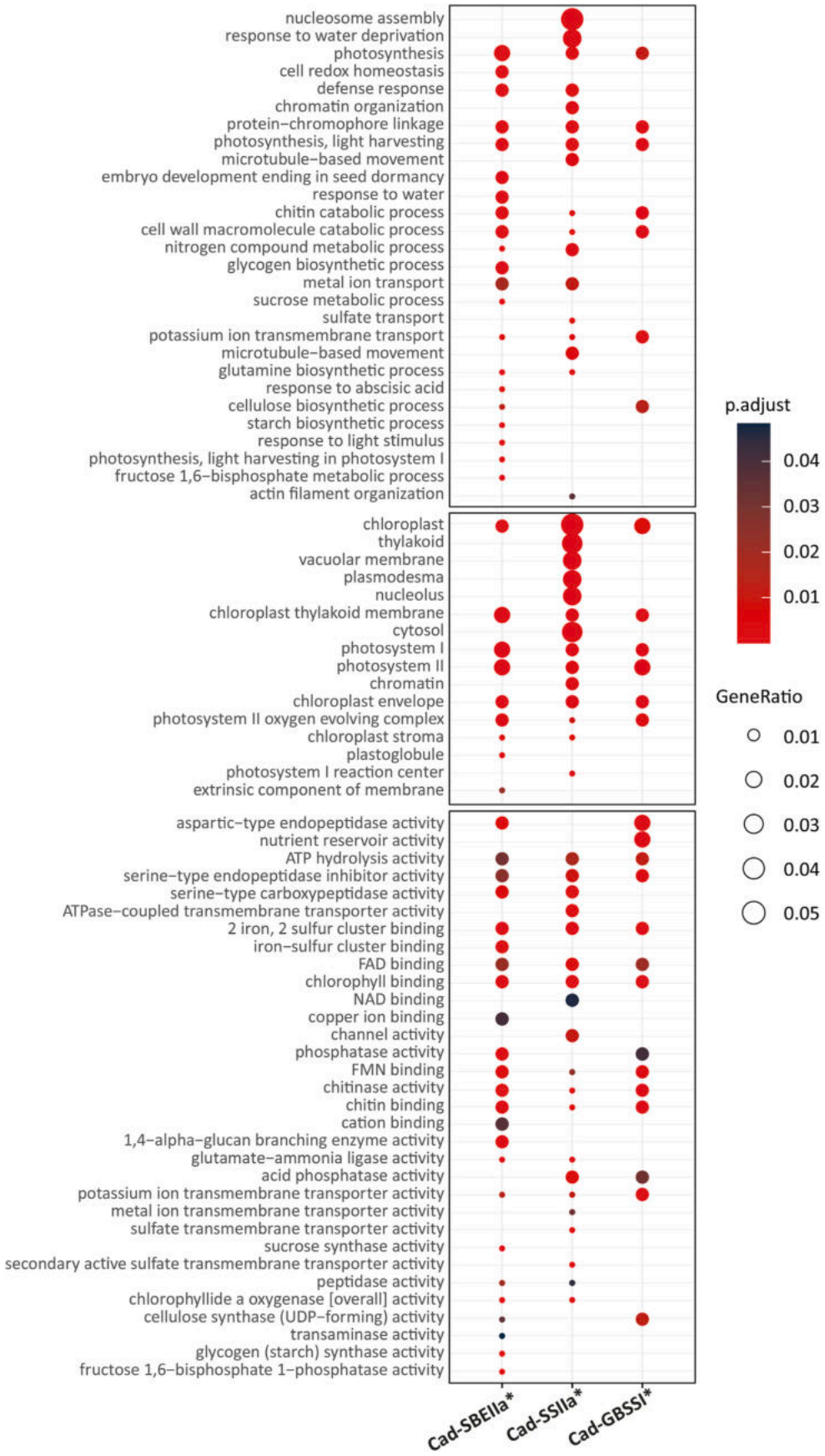


(caption on next page)

**Fig. 2.** Gene Ontology (GO) enrichment analysis of DEGs. The GO terms (y-axis) were grouped into boxes according to biological process (upper box), cell compartment (middle box), and molecular function (lower box) categories. Dot size represents the number of DEGs per class over the total DEGs number (gene ratio) found in each genotype (x-axis). Color gradation from blue (lower significance) to red (higher significance) represents adjusted *p*-value (*p*.adjust) according to Benjamini-Hochberg procedure.

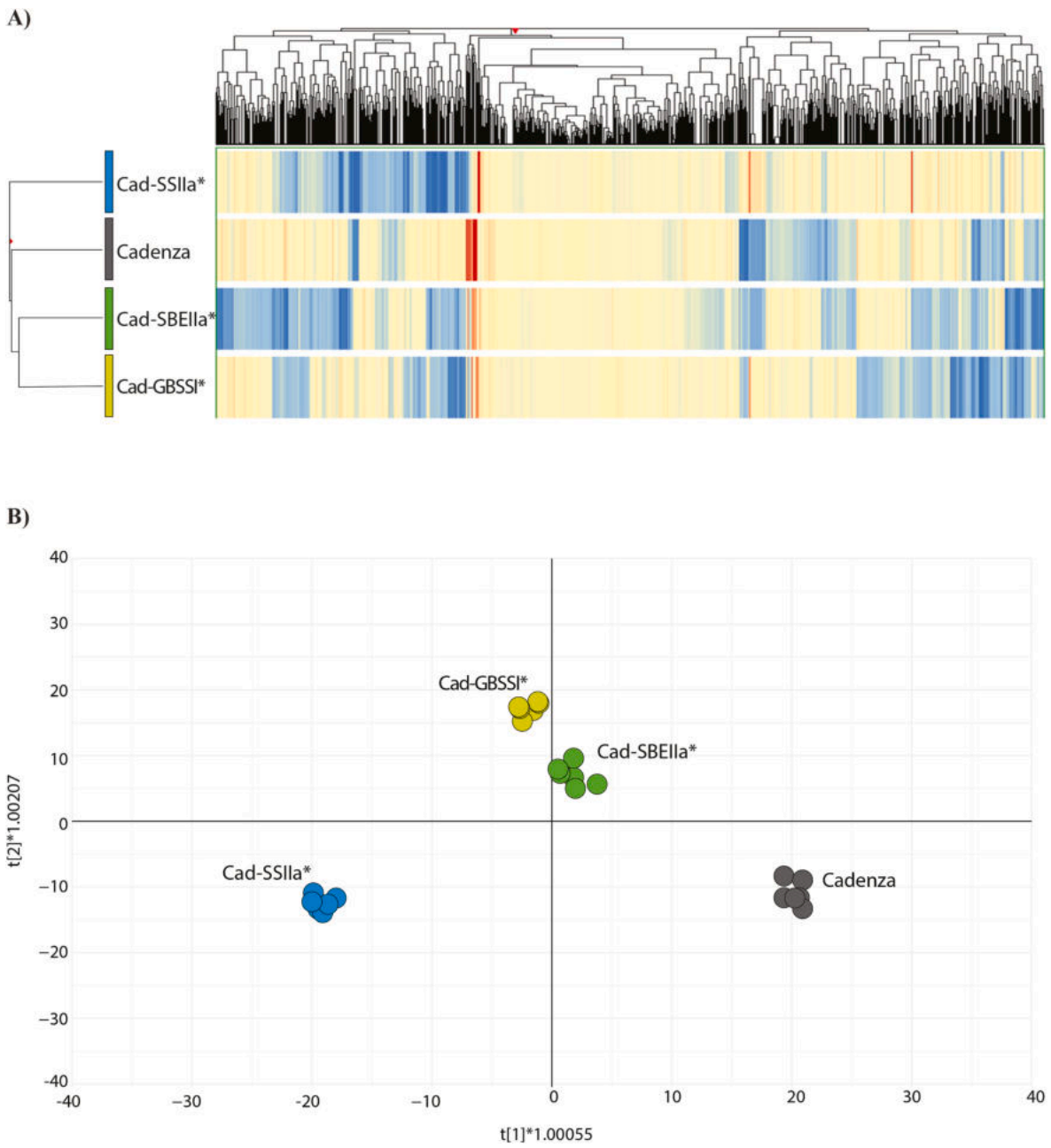


**Fig. 3.** Untargeted metabolic fingerprinting of grains from mutant genotypes. Metabolomics profiling of the dataset (1758 compounds) annotated by UHPLC-QTOF/MS from grain samples of high-amylose genotypes (Cad-GBSSI*, Cad-SSIIa* and Cad-SBEIIa*) and the wild type plants (Cadenza). (A) Hierarchical cluster analysis (HCA) of metabolomics data. The fold-change based heatmap was built on normalized intensities and samples were clustered according to Ward's algorithm, based on Euclidean distances matrix. (B) Score plot of orthogonal projection to latent structures discriminant analysis (OPLS-DA) supervised modelling (R2Y 0.99, Q2Y 0.92). The ellipse shown in the model represents the Hotelling T2 with 95% confidence. The total number of replicates (n = 6) accounts for 2 technical replications for each biological replicate (n = 3).

immature kernels of the four genotypes were investigated by TEM. Overall, TEM analysis showed significant differences in the number of starch granules inside the chloroplast among the genotypes. In the WT, the chloroplast structure was recurrent as elliptical with well-organized thylakoids into regular grana and containing few starch grains and plastoglobules (Fig. 5A-C). Pericarp cells of Cad-GBSSI* showed no evident ultrastructure alterations (Fig. 5D–F) though a higher number of starch granules and plastoglobules was observed *vs* WT (Fig. 6). Similarly, Cad-SSIIa* showed an unaltered chloroplast shape but dilation of the thylakoid lumina was evident (Fig. 5G–I) as well as a slightly greater number of starch grains (Fig. 6). Cad-SBEIIa* chloroplasts were affected by severe changes (Fig. 5J-N) since most of them lost the elliptical shape

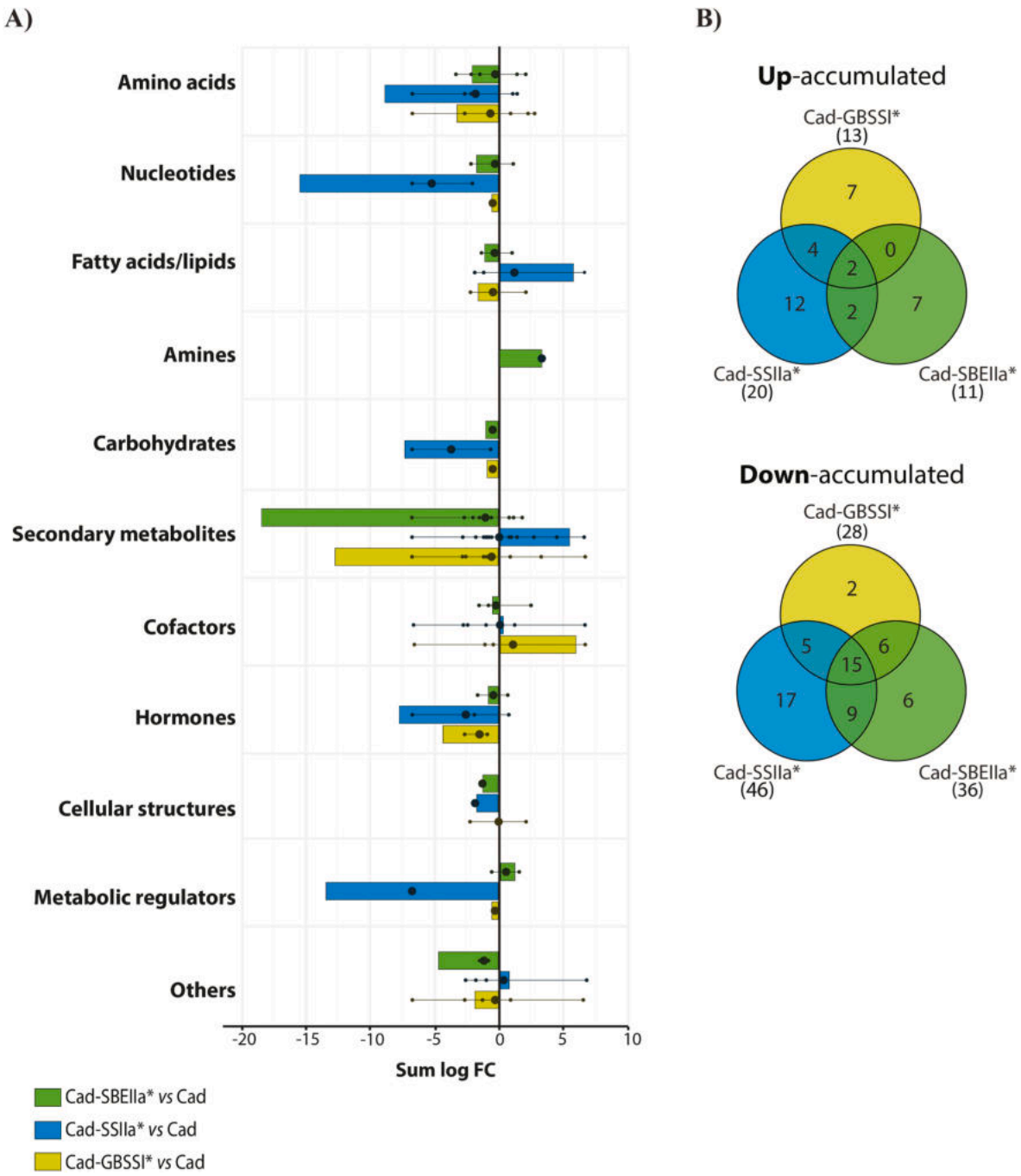


**Fig. 4.** Metabolic pathways depicted by differentially modulated metabolites. (A) Differential metabolites of mutant genotypes (Cad-GBSSI*, Cad-SSIIa*, and Cad-SBEIIa*) *vs* wild type (Cadenza). Within each class of compounds (y-axis), large and small dots indicate respectively the mean log fold change (FC) of all metabolites and the individual log FC of every metabolite. The extent of the colored bars corresponds to the sum of all data values for metabolites within the different compound classes. The x-axis corresponds to the cumulative log fold change (sum log FC). (B) Venn diagram showing the number of metabolites specifically up- and down-accumulated in each mutant.

and were aberrant (Fig. 5J and K) and notably enlarged (Fig. 6F). Specifically, the thylakoid membrane system was disorganized as well as the thylakoid grana stacking together with a very dense stroma and starch grains with irregular shape. Finally, the number of plastoglobules increased and their distribution was randomly distributed within the chloroplast (Fig. 5J and K; Fig. 6). Furthermore, amyloplasts in Cad-SSIIa* and Cad-SBEIIa* showed aberrant shapes and the emergence of empty stromal volumes (Fig. S3), emphasizing the impact on amyloplast ultrastructure in these two genotypes.

### 3.6. DEGs subtending chloroplast phenotypes

In order to reconstruct the genetic events that might be involved in the phenotypic differences observed in mutants, 4873 plastid-related genes were identified and classified into 18 functional categories accounting for structural (chloroplast biogenesis, thylakoid architecture, etc.) and functional (metabolism, photosynthesis, etc.) roles (Fig. 7A and Table S10). Overall, 425 of these genes were differentially regulated, with the number of down-tuned ones exceeding those of up-regulated genes. Cad-SBEIIa* showed the highest number of DEGs (312),

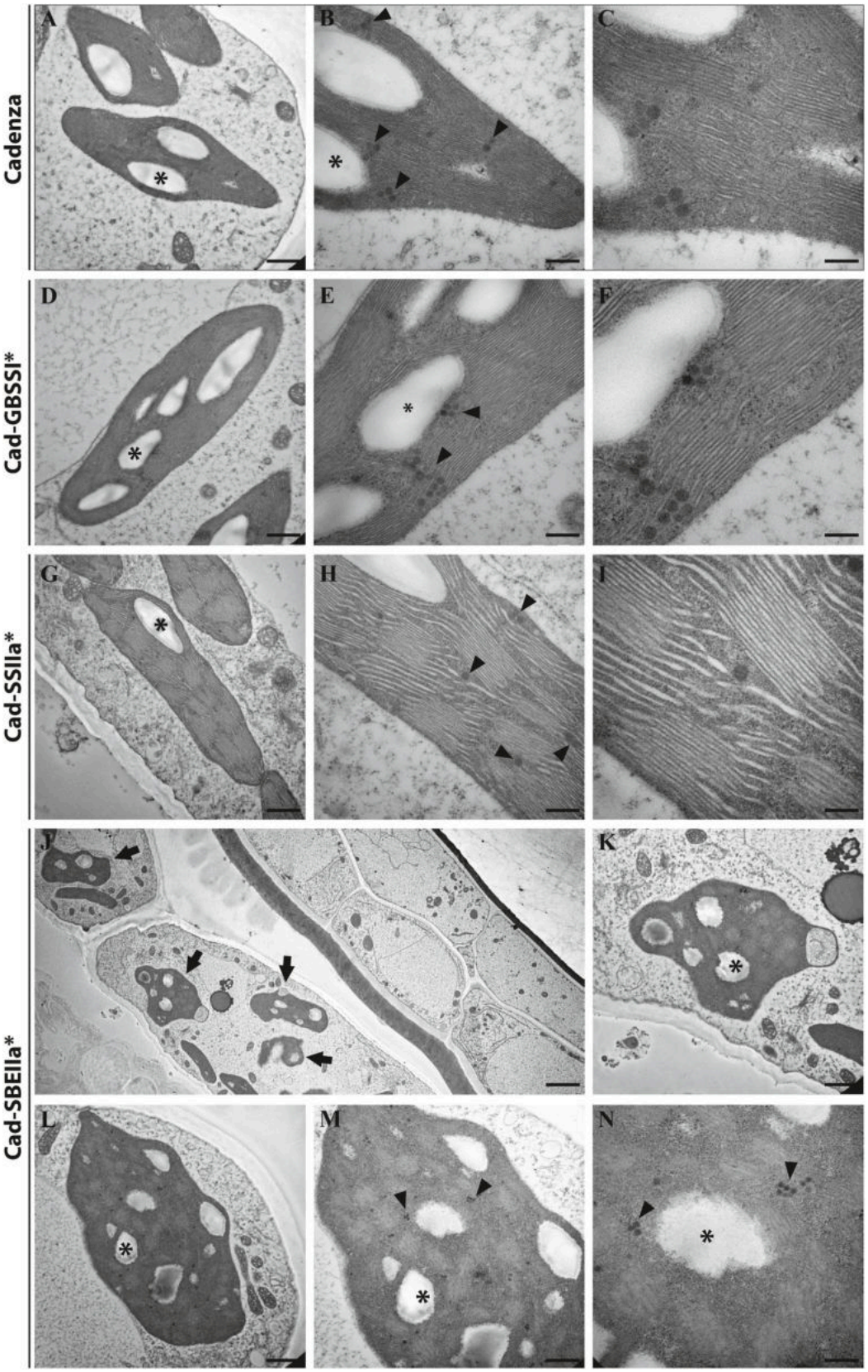


**Fig. 5.** Ultrastructure of pericarp chloroplasts in mutant and wild type immature grains (25 dpa). Electron micrographs of Cadenza wild type (A–C), Cad-GBSSI* (D–F), Cad-SSIIa* (G–I), and Cad-SBEIIa* (J–N). Asterisk, starch grains; arrows, aberrant chloroplasts; arrowheads, plastoglobules. Bar sizes: 10 μm in J; 2 μm in K, L, G; 1 μm in A, D, M; 500 nm in B, E, H, N; 200 nm in C, F, I. In J at right, tube cells; all the chloroplasts are located in the cross cells at left.

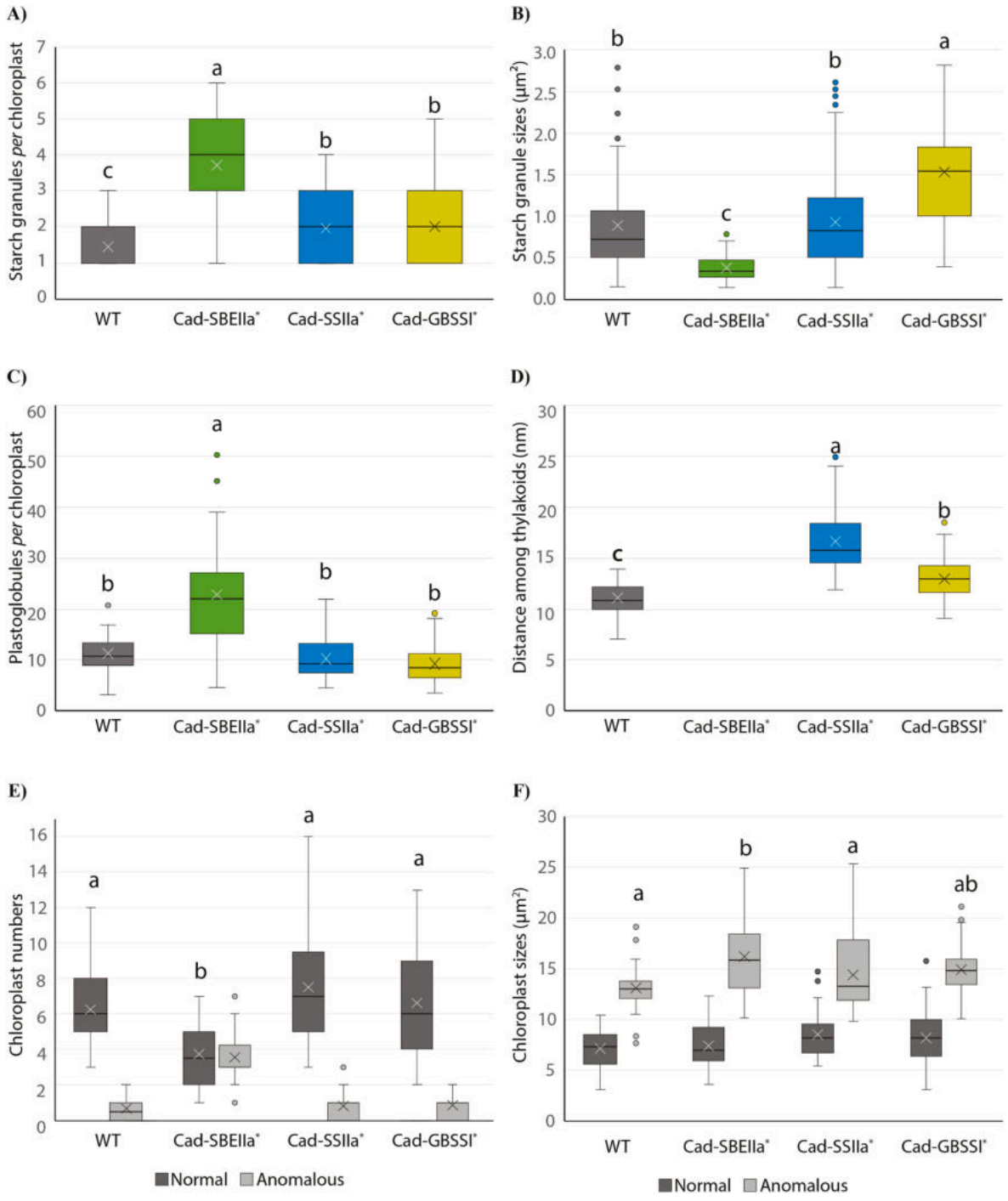


**Fig. 6.** Box plots of chloroplast measurements in mutant and control immature kernels (25 dpa). Medians are marked by horizontal bars within each box; boxes span from the 25th to the 75th percentile of each group's distribution of value. Outliers (if any) are shown by dots. Different letters indicate statistically significant differences according to ANOVA with the Tukey HSD test, $p < 0.01$.

followed by Cad-SSIIa* (252), and Cad-GBSSI* (125), and a proportion of 42 %, 34 %, and 15 % were specifically altered in each line (Fig. 7B). DEGs enrichment analyses revealed that the 'photosynthesis' group was commonly perturbed in all mutants, the 'redox' category was altered in both Cad-SBEIIa* and Cad-SSIIa*, and the 'senescence' and 'thylakoid architecture' groups were specifically enriched in Cad-SBEIIa* (Fig. 7C). Most of the DEGs enriched in the above-said categories were down-regulated in the different genotypes (Fig. 7D). Moreover, addressing *amylase* expression patterns highlighted that starch degradation may have been altered through different mechanisms in the three mutants. Indeed, Cad-SSIIa* and Cad-GBSSI* were affected (down-tuned) in distinct alpha-amylase classes, while Cad-SBEIIa* showed specific down-regulation of beta-amylases known to be active in chloroplasts (Fig. 7D). Taken together, functional DEGs are consistent with the supposed process of chloroplast dismantling as observed in TEM analyses.

## 4. Discussion

Metabolic engineering of starch biosynthesis is a powerful technology to produce crops with altered amylose/amylopectin ratios and improved starch properties tailored to benefit human health (Xia et al.,

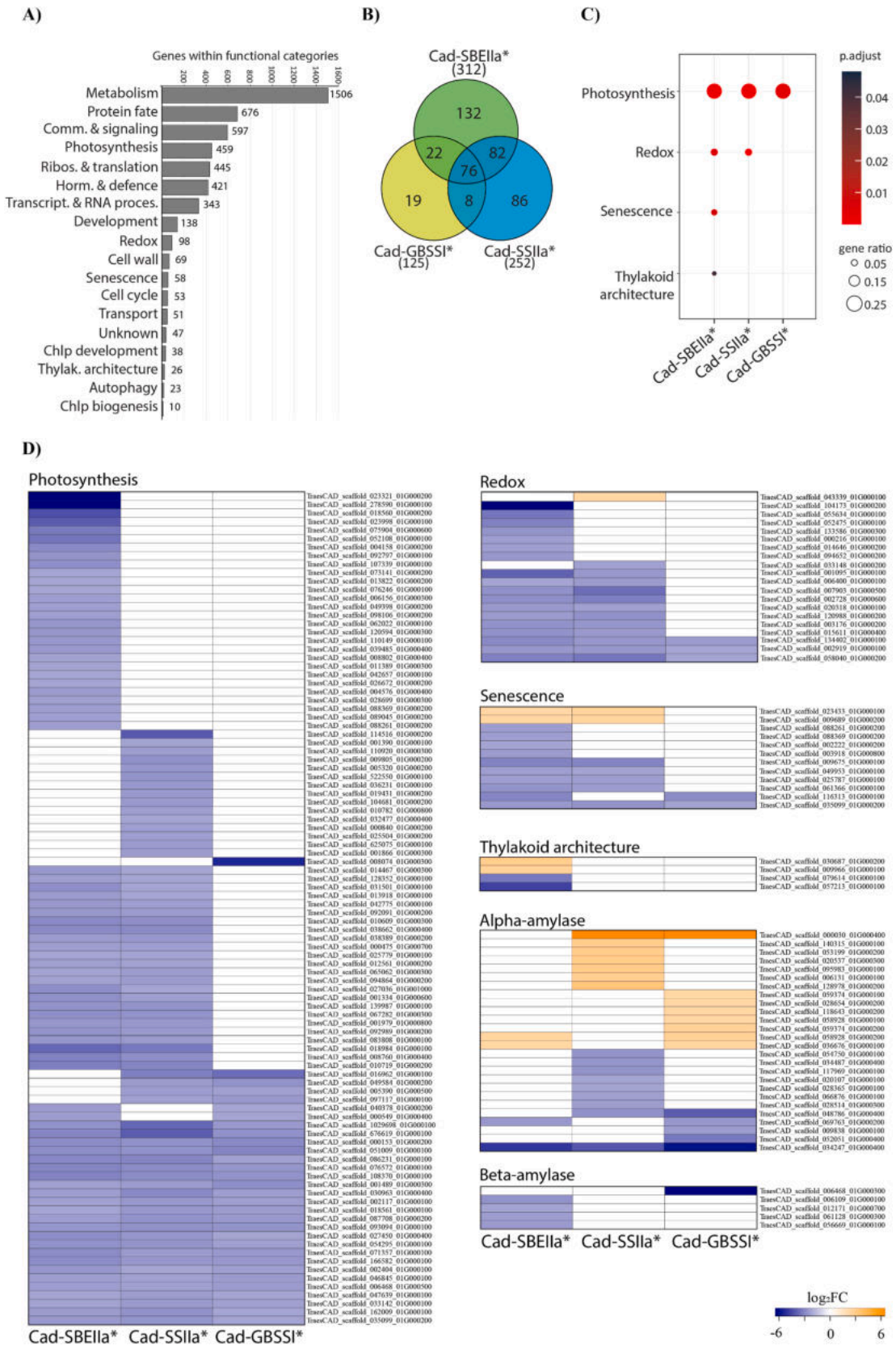


**Fig. 7.** Enrichment of functional categories. (A) Bar chart showing the distribution of plastid-related genes into 18 functional categories. (B) Venn diagram of specific and shared plastid-related DEGs. The total number of DEGs per genotype is in brackets. (C) Dot plot of functional categories enriched with plastid-related DEGs. (D) Expression profile heat maps of DEGs enriching the functional categories ('photosynthesis', 'senescence', 'redox', and 'thylakoid architecture') or within the alpha- and beta-amylases groups. The color gradients refer to values of log2FC in mutant *vs* WT comparisons where orange and blue indicate up- and downregulation, respectively.

2018). In cereal grains, a plethora of genes have been targeted either to understand their function or to develop new genotypes with improved nutritional and technological value (Xia et al., 2018; Wang et al., 2017; Irshad et al., 2021), but less is known about the plant metabolic response to changes in starch composition. Comprehensive characterization of starch mutants is therefore essential to monitor effects in addition to those expected from genetic modifications. Unintended pleiotropic effects have often been associated with different mutations affecting the starch synthesis in different cereal species. The effects included deregulation of enzymes in the starch or other metabolic pathways (e.g. carbon allocation and partitioning) and phenotypic traits, such as lower starch content, reduced yield, shrunken kernel (Sparla et al., 2014; Fujita et al., 2022; Zhang et al., 2020). A few works addressed the impact on seedling development caused by changing the reserve starch and its turnover (Carciofi et al., 2012). Furthermore, the effects of changes in starch structure have been less explored compared to those of starch biosynthesis, excess, or shortage, mainly addressed in leaves (Ragel et al., 2013; Sparla et al., 2014; Chen et al., 2022; Hausler et al., 2009). Here, wheat mutants (with a common varietal background) with extreme phenotypes of starch branching and amylose content were effective to study plant responses to starch structural changes. Ultrastructural and omics analyses focused on immature caryopses of previously described starch mutant lines (Botticella et al., 2018) and shed light on gene-metabolite networks acting on starch metabolism. The integration of the analysis revealed that each gene-specific mutation caused common downstream modifications and specific regulatory mechanisms likely to subtend phenotypic differences. From here on, data will be discussed by pinpointing common and distinctive aspects among the three mutants.

The highest transcriptomic divergence in Cad-SSIIa* and Cad-SBEIIa* compared to the wild type (Fig. 1) was consistent with the greatest differences in kernel and starch traits. The transcriptome patterns (Fig. S2) were comparable to previous work (Botticella et al., 2011, 2018), including the compensatory up-regulation of starch biosynthetic genes other than the mutated ones observed in bread and durum wheat starch mutant lines (Hogg et al., 2013; Sestili et al., 2010b; Yang et al., 2022). Accordingly, the expression of upstream biosynthetic genes (Fig. S2) sustained carbon reallocation mechanisms throughout the metabolic network (e.g. *SUS, HK,* and *Bt*). Enrichment analysis pointed to mutant-specific side effects that included plastid-related genes (Fig. 2). In parallel, the altered levels of compounds in the chlorophyll, tocopherol, quinol, and quinone pathways supported the effects on chloroplasts (Table S9). Moreover, it is known that tocopherols biosynthesis takes place in the chloroplast envelope and in thylakoid-linked plastoglobules, exerting functions in membrane photoprotection, integrity and functionality (Morelli et al., 2023). In this context, the enrichment analyses at the transcriptomic (e.g. chloroplast envelope and thylakoid membrane GO terms, Fig. 2) and metabolic levels (tocopherol biosynthesis, Table S9) converged to support that wheat mutants shared alterations in chloroplast membranes; ultrastructural analyses further confirmed that modifications affected chloroplasts in the kernel pericarp (Fig. 5). The effects on chloroplast elements (e.g. thylakoids and stroma) and plastoglobules increased in intensity from Cad-GBSSI* to Cad-SBEIIa* (Fig. 6); this observation is consistent with the amylose percentage previously measured in these mutants (Botticella et al., 2018). Inherently, the altered composition of starch was proposed to affect (directly or indirectly) chloroplast organization and function in maize leaves (Yandeau-Nelson et al., 2011). Specifically, the observed enlargement of the thylakoid lumen, coupled with the presence of several differentially expressed genes (DEGs) associated with photosynthetic systems in CadSSIIa* (Figs. 6 and 7), is consistent with the essential role of SSIIa in interacting with the thylakoid membrane, a crucial step in achieving proper starch assembly (Gamez-Arjona et al., 2014). Altering SSIIa and SBEIIa key enzymes in the amylopectin route affected the pericarp chloroplast, which is the site of seed photosynthesis. However, measuring photosynthesis efficiency in kernels - a debated matter and a technical challenge (Henry et al., 2017) - was beyond the scope of this work, although the enrichment of DEGs in both mutants places photosynthesis at the top of the list of altered functional categories in both mutants (Fig. 7). Focusing on Cad-SBEIIa*, the chloroplast alterations scored in kernels (aberrant/enlarged shape, inner membrane disorganization, grana stacking alteration, and plastoglobule increased number, Figs. 5 and 6) recalled those described in leaf chloroplast degeneration (Mulisch et al., 2013). Moreover, starch-accumulating leaves of *SBEIIa* maize mutants showed impairment of photosynthesis and carbohydrate availability at night, leading to premature chloroplast senescence (Yandeau-Nelson et al., 2011). Here, starch accumulation in pericarp chloroplast of Cad-SBEIIa* was associated with acceleration in chloroplast senescence. The impact of starch accumulation on chloroplast function (Yandeau-Nelson et al., 2011) is substantiated in wheat pericarp by two significant events. The first consists in the contribution of misregulated *CURVATURE THYLAKOID1* genes (Fig. 7) to the altered grana organization (Fig. 5) (Dominguez and Cejudo, 2021). The downregulation of *CURT* genes in Cad-SBEIIa* is closely linked to the hyperstacking of grana thylakoids (due to the repulsion among phosphate heads that modulate grana spatial organization) as demonstrated in functional studies (Sandoval-Ibáñez et al., 2021; Trotta et al., 2019). Secondly, a general down-regulation of β-amylases in cadenza mutants (Fig. 7) sustains a reduced amylase-driven degradation of high-amylose starch. Taken together, the above-mentioned events are likely to harsh the natural oxidative stress occurring in the chloroplast (Khatoon et al., 2009), leading to ROS accumulation, as supported by the DEGs enrichment of redox terms. Indeed, ROS accumulation is a hallmark of the chloroplast-to-gerontoplast transition, together with the accumulation of plastoglobules (Fig. 6), which is characteristic of Cad-SBEIIa* chloroplasts. Interestingly, in Cad-SBEIIa* seeds, the profound reduction in branched glucan chains reproduced a scenario very close to what was observed in the leaf of a SBEIIa maize mutant, pointing at the importance of all green tissues, other than the leaf, in the photosynthetic process. The poor grade of branching makes starch less susceptible to hydrolysis slowing down all metabolism, sequestering substrate (building block, ADP-glucose) for metabolites biosynthesis and inducing oxidative stress, proved by the increased number of plastoglobules and antioxidant compounds.

## Funding

The research was funded by the Ministry for Education, University, and Research (MIUR) initiative "Department of Excellence" (Law 232/2016) DAFNE Project 2023-27 "Digital, Intelligent, Green and Sustainable (acronym: D.I.Ver.So.).

## CRediT authorship contribution statement

**Ermelinda Botticella:** Data curation, Writing – original draft. **Giulio Testone:** Data curation, Formal analysis, Validation, Writing – original draft. **Valentina Buffagni:** Formal analysis, Writing – original draft, Data curation. **Samuela Palombieri:** Data curation, Formal analysis, Writing – review & editing. **Anna Rita Taddei:** Formal analysis, Methodology. **Domenico Lafiandra:** Writing – review & editing. **Luigi Lucini:** Data curation, Validation, Writing – review & editing. **Donato Giannino:** Conceptualization, Validation, Writing – original draft. **Francesco Sestili:** Conceptualization, Funding acquisition, Writing – original draft.

## Declaration of competing interest

The authors declare that they have no known competing financial interests or personal relationships that could have appeared to influence the work reported in this paper.

## Data availability

Data will be made available on request.

## Acknowledgements

The authors thank the "Romeo ed Enrica Invernizzi" foundation (Milan, Italy), for its kind support to the metabolomics facility at Università Cattolica del Sacro Cuore; the Department of Plant Science Rothamstead Research Harpenden UK that provided the original wheat mutants.

## Appendix A. Supplementary data

Supplementary data to this article can be found online at https://doi.org/10.1016/j.plaphy.2024.108354.

## References

Bolger, A.M., Lohse, M., Usadel, B., 2014. Trimmomatic: a flexible trimmer for Illumina sequence data. Bioinformatics 30, 2114–2120. https://doi.org/10.1093/bioinformatics/btu170.

Botticella, E., Sestili, F., Hernandez-Lopez, A., Phillips, A., Lafiandra, D., 2011. High resolution melting analysis for the detection of EMS induced mutations in wheat SBEIIa genes. BMC Plant Biol. 11, 156. https://doi.org/10.1186/1471-2229-11-156.

Botticella, E., Sestili, F., Sparla, F., Moscatello, S., Marri, L., Cuesta-Seijo, J.A., Falini, G., Battistelli, A., Trost, P., Lafiandra, D., 2018. Combining mutations at genes encoding key enzymes involved in starch synthesis affects the amylose content, carbohydrate allocation and hardness in the wheat grain. Plant Biotechnol. J. 16, 1723–1734. https://doi.org/10.1111/pbi.12908.

Botticella, E., Savatin, D.V., Sestili, F., 2021. The triple jags of dietary fibers in cereals: how biotechnology is longing for high fiber grains. Front. Plant Sci. 12, 745579 https://doi.org/10.3389/fpls.2021.745579.

Buffagni, V., Zhang, L., Senizza, B., Rocchetti, G., Ferrarini, A., Miras-Moreno, B., Lucini, L., 2022. Metabolomics and lipidomics insight into the effect of different polyamines on tomato plants under non-stress and salinity conditions. Plant Sci. 322, 111346 https://doi.org/10.1016/j.plantsci.2022.111346.

Carciofi, M., Blennow, A., Jensen, S.L., Shaik, S.S., Henriksen, A., Buleon, A., Holm, P.B., Hebelstrup, K.H., 2012. Concerted suppression of all starch branching enzyme genes in barley produces amylose-only starch granules. BMC Plant Biol. 12, 223. https://doi.org/10.1186/1471-2229-12-223.

Caspi, R., Dreher, K., Karp, P.D., 2013. The challenge of constructing, classifying, and representing metabolic pathways. FEMS Microbiol. Lett. 345, 85–93. https://doi.org/10.1111/1574-6968.12194.

Chen, X., Chen, M., Lin, G., Yang, Y., Yu, X., Wu, Y., Xiong, F., 2019. Structural development and physicochemical properties of starch in caryopsis of super rice with different types of panicle. BMC Plant Biol. 19, 482. https://doi.org/10.1186/s12870-019-2101-7.

Chen, Z., Wang, Y., Huang, R., Zhang, Z., Huang, J., Yu, F., Lin, Y., Guo, Y., Liang, K., Zhou, Y., Chen, F., 2022. Integration of transcriptomic and proteomic analyses reveals several levels of metabolic regulation in the excess starch and early senescent leaf mutant lses1 in rice. BMC Plant Biol. 22, 137. https://doi.org/10.1186/s12870-022-03510-2.

Choi, H., Yi, T., Ha, S.H., 2021. Diversity of plastid types and their interconversions. Front. Plant Sci. 12, 692024 https://doi.org/10.3389/fpls.2021.692024.

Dominguez, F., Cejudo, F.J., 2021. Chloroplast dismantling in leaf senescence. J. Exp. Bot. 72, 5905–5918. https://doi.org/10.1093/jxb/erab200.

Fujita, N., Miura, S., Crofts, N., 2022. Effects of various allelic combinations of starch biosynthetic genes on the properties of endosperm starch in rice. Rice 15, 24. https://doi.org/10.1186/s12284-022-00570-8.

Gamez-Arjona, F.M., Raynaud, S., Ragel, P., Merida, A., 2014. Starch synthase 4 is located in the thylakoid membrane and interacts with plastoglobule-associated proteins in Arabidopsis. Plant J. 80, 305–316. https://doi.org/10.1111/tpj.12633.

Ganugi, P., Fiorini, A., Ardenti, F., Caffi, T., Bonini, P., Taskin, E., Puglisi, E., Tabaglio, V., Trevisan, M., Lucini, L., 2022. Nitrogen use efficiency, rhizosphere bacterial community, and root metabolome reprogramming due to maize seed treatment with microbial biostimulants. Physiol. Plantarum 174, e13679. https://doi.org/10.1111/ppl.13679.

Gu, Y., Han, S., Chen, L., Mu, J., Duan, L., Li, Y., Yan, Y., Li, X., 2021. Expression and regulation of genes involved in the reserve starch biosynthesis pathway in hexaploid wheat (Triticum aestivum L.). Crop J. 9, 440–455. https://doi.org/10.1016/j.cj.2020.08.002.

Hausler, R.E., Geimer, S., Kunz, H.H., Schmitz, J., Dormann, P., Bell, K., Hetfeld, S., Guballa, A., Flugge, U.I., 2009. Chlororespiration and grana hyperstacking: how an Arabidopsis double mutant can survive despite defects in starch biosynthesis and daily carbon export from chloroplasts. Plant Physiol. 149, 515–533. https://doi.org/10.1104/pp.108.128124.

Hawkins, C., Ginzburg, D., Zhao, K., Dwyer, W., Xue, B., Xu, A., Rice, S., Cole, B., Paley, S., Karp, P., Rhee, S.Y., 2021. Plant Metabolic Network 15: a resource of genome-wide metabolism databases for 126 plants and algae. J. Integr. Plant Biol. 63, 1888–1905. https://doi.org/10.1111/jipb.13163.

Henry, R.J., Rangan, P., Furtado, A., Busch, F.A., Farquhar, G.D., 2017. Does C(4) photosynthesis occur in wheat seeds? Plant Physiol. 174, 1992–1995. https://doi.org/10.1104/pp.17.00837.

Hogg, A.C., Gause, K., Hofer, P., Martin, J.M., Graybosch, R.A., Hansen, L.E., Giroux, M. J., 2013. Creation of a high-amylose durum wheat through mutagenesis of starch synthase II (SSIIa). J. Cereal. Sci. 57, 377–383. https://doi.org/10.1016/j.jcs.2013.01.001.

Huang, L., Tan, H., Zhang, C., Li, Q., Liu, Q., 2021. Starch biosynthesis in cereal endosperms: an updated review over the last decade. Plant Commun. 2, 100237 https://doi.org/10.1016/j.xplc.2021.100237.

Irshad, A., Guo, H., Rehman, S.U., Wang, X., Wang, C., Raza, A., Zhou, C., Li, Y., Liu, L., 2021. Soluble starch synthase enzymes in cereals: an updated review. Agronomy 11, 1983.

James, M.G., Denyer, K., Myers, A.M., 2003. Starch synthesis in the cereal endosperm. Curr. Opin. Plant Biol. 6, 215–222. https://doi.org/10.1016/s1369-5266(03)00042-6.

Khatoon, M., Inagawa, K., Pospíšil, P., Yamashita, A., Yoshioka, M., Lundin, B., Horie, J., Morita, N., Jajoo, A., Yamamoto, Y., Yamamoto, Y., 2009. Quality control of photosystem II: thylakoid unstacking is necessary to avoid further damage to the D1 protein and to facilitate D1 degradation under light stress in spinach thylakoids. J. Biol. Chem. 284, 25343–25352. https://doi.org/10.1074/jbc.M109.007740.

Kim, D., Paggi, J.M., Park, C., Bennett, C., Salzberg, S.L., 2019. Graph-based genome alignment and genotyping with HISAT2 and HISAT-genotype. Nat. Biotechnol. 37, 907–915. https://doi.org/10.1038/s41587-019-0201-4.

Kong, L.A., Xie, Y., Sun, M.Z., Si, J.S., Hu, L., 2016. Comparison of the photosynthetic characteristics in the pericarp and flag leaves during wheat (Triticum aestivum L.) caryopsis development. Photosynthetica 54, 40–46. https://doi.org/10.1007/s11099-015-0153-y.

Loudya, N., Mishra, P., Takahagi, K., Uehara-Yamaguchi, Y., Inoue, K., Bogre, L., Mochida, K., Lopez-Juez, E., 2021. Cellular and transcriptomic analyses reveal two-staged chloroplast biogenesis underpinning photosynthesis build-up in the wheat leaf. Genome Biol. 22, 151. https://doi.org/10.1186/s13059-021-02366-3.

Love, M.I., Huber, W., Anders, S., 2014. Moderated estimation of fold change and dispersion for RNA-seq data with DESeq2. Genome Biol. 15, 550. https://doi.org/10.1186/s13059-014-0550-8.

MacNeill, G.J., Mehrpouyan, S., Minow, M.A.A., Patterson, J.A., Tetlow, I.J., Emes, M.J., 2017. Starch as a source, starch as a sink: the bifunctional role of starch in carbon allocation. J. Exp. Bot. 68, 4433–4453. https://doi.org/10.1093/jxb/erx291.

Martin, M., 2011. Cutadapt removes adapter sequences from high-throughput sequencing reads,. No 1: Next Generation Sequencing Data AnalysisDO EMBnet J. 17. https://doi.org/10.14806/ej.17.1.200.

Morelli, L., Garcia Romanach, L., Glauser, G., Shanmugabalaji, V., Kessler, F., Rodriguez-Concepcion, M., 2023. Nutritional enrichment of plant leaves by combining genes promoting tocopherol biosynthesis and storage. Metabolites 13. https://doi.org/10.3390/metabo13020193.

Mulisch, M., Krupinska, K., 2013. Ultrastructural analyses of senescence associated dismantling of chloroplasts revisited. In: Biswal, B., Krupinska, K., Biswal, U.C. (Eds.), Plastid Development in Leaves during Growth and Senescence. Springer Netherlands, Dordrecht, pp. 307–335.

Pertea, M., Pertea, G.M., Antonescu, C.M., Chang, T.C., Mendell, J.T., Salzberg, S.L., 2015. StringTie enables improved reconstruction of a transcriptome from RNA-seq reads. Nat. Biotechnol. 33, 290–295. https://doi.org/10.1038/nbt.3122.

Pfister, B., Zeeman, S.C., 2016. Formation of starch in plant cells. Cell. Mol. Life Sci. 73, 2781–2807. https://doi.org/10.1007/s00018-016-2250-x.

Ragel, P., Streb, S., Feil, R., Sahrawy, M., Annunziata, M.G., Lunn, J.E., Zeeman, S., Merida, A., 2013. Loss of starch granule initiation has a deleterious effect on the growth of arabidopsis plants due to an accumulation of ADP-glucose. Plant Physiol. 163, 75–85. https://doi.org/10.1104/pp.113.223420.

Salek, R.M., Neumann, S., Schober, D., Hummel, J., Billiau, K., Kopka, J., Correa, E., Reijmers, T., Rosato, A., Tenori, L., Turano, P., Marin, S., Deborde, C., Jacob, D., Rolin, D., Dartigues, B., Conesa, P., Haug, K., Rocca-Serra, P., O'Hagan, S., Hao, J., van Vliet, M., Sysi-Aho, M., Ludwig, C., Bouwman, J., Cascante, M., Ebbels, T., Griffin, J.L., Moing, A., Nikolski, M., Oresic, M., Sansone, S.A., Viant, M.R., Goodacre, R., Gunther, U.L., Hankemeier, T., Luchinat, C., Walther, D., Steinbeck, C., 2015. COordination of Standards in MetabOlomicS (COSMOS): facilitating integrated metabolomics data access. Metabolomics 11, 1587–1597. https://doi.org/10.1007/s11306-015-0810-y.

Sandoval-Ibáñez, O., Sharma, A., Bykowski, M., Borràs-Gas, G., Behrendorff, J.B.Y.H., Mellor, S., Qvortrup, K., Verdonk, J.C., Bock, R., Kowalewska, Ł., Pribil, M., 2021. Curvature thylakoid 1 proteins modulate prolamellar body morphology and promote organized thylakoid biogenesis in Arabidopsis thaliana. Proc. Natl. Acad. Sci. USA 118, e2113934118. https://doi.org/10.1073/pnas.2113934118.

Sestili, F., Botticella, E., Bedo, Z., Phillips, A., Lafiandra, D., 2010a. Production of novel allelic variation for genes involved in starch biosynthesis through mutagenesis. Mol. Breed. 25, 145–154. https://doi.org/10.1007/s11032-009-9314-7.

Sestili, F., Janni, M., Doherty, A., Botticella, E., D'Ovidio, R., Masci, S., Jones, H.D., Lafiandra, D., 2010b. Increasing the amylose content of durum wheat through silencing of the SBEIIa genes. BMC Plant Biol. 10, 144. https://doi.org/10.1186/1471-2229-10-144.

Sparla, F., Falini, G., Botticella, E., Pirone, C., Talamè, V., Bovina, R., Salvi, S., Tuberosa, R., Sestili, F., Trost, P., 2014. New starch phenotypes produced by TILLING in barley. PLoS One 9, e107779. https://doi.org/10.1371/journal.pone.0107779.

Tetlow, I.J., Morell, M.K., Emes, M.J., 2004. Recent developments in understanding the regulation of starch metabolism in higher plants. J. Exp. Bot. 55, 2131–2145. https://doi.org/10.1093/jxb/erh248.

Trotta, A., Bajwa, A.A., Mancini, I., Paakkarinen, V., Pribil, M., Aro, E.-M., 2019. The role of phosphorylation dynamics of CURVATURE THYLAKOID 1B in plant thylakoid Membranes1 [OPEN]. Plant Physiol. 181, 1615–1631. https://doi.org/10.1104/pp.19.00942.

Vrinten, P.L., Nakamura, T., 2000. Wheat granule-bound starch synthase I and II are encoded by separate genes that are expressed in different tissues. Plant Physiol. 122, 255–264. https://doi.org/10.1104/pp.122.1.255.

Wang, J., Hu, P., Chen, Z., Liu, Q., Wei, C., 2017. Progress in high-amylose cereal crops through inactivation of starch branching enzymes. Front. Plant Sci. 8, 469. https://doi.org/10.3389/fpls.2017.00469.

Wu, T., Hu, E., Xu, S., Chen, M., Guo, P., Dai, Z., Feng, T., Zhou, L., Tang, W., Zhan, L., Fu, X., Liu, S., Bo, X., Yu, G., 2021. clusterProfiler 4.0: a universal enrichment tool for interpreting omics data. Innovation 2, 100141. https://doi.org/10.1016/j.xinn.2021.100141.

Xia, J., Zhu, D., Wang, R., Cui, Y., Yan, Y., 2018. Crop resistant starch and genetic improvement: a review of recent advances. Theor. Appl. Genet. 131, 2495–2511. https://doi.org/10.1007/s00122-018-3221-4.

Xiong, F., Yu, X.R., Zhou, L., Wang, F., Xiong, A.S., 2013. Structural and physiological characterization during wheat pericarp development. Plant Cell Rep. 32, 1309–1320. https://doi.org/10.1007/s00299-013-1445-y.

Yandeau-Nelson, M.D., Laurens, L., Shi, Z., Xia, H., Smith, A.M., Guiltinan, M.J., 2011. Starch-branching enzyme IIa is required for proper diurnal cycling of starch in leaves of maize. Plant Physiol. 156, 479–490. https://doi.org/10.1104/pp.111.174094.

Yang, Q., Ding, J., Feng, X., Zhong, X., Lan, J., Tang, H., Harwood, W., Li, Z., Guzmán, C., Xu, Q., Zhang, Y., Jiang, Y., Qi, P., Deng, M., Ma, J., Wang, J., Chen, G., Lan, X., Wei, Y., Zheng, Y., Jiang, Q., 2022. Editing of the starch synthase IIa gene led to transcriptomic and metabolomic changes and high amylose starch in barley. Carbohydr. Polym. 285, 119238 https://doi.org/10.1016/j.carbpol.2022.119238.

Yu, X., Li, B., Wang, L., Chen, X., Wang, W., Wang, Z., Xiong, F., 2015. Systematic analysis of pericarp starch accumulation and degradation during wheat caryopsis development. PLoS One 10, e0138228. https://doi.org/10.1371/journal.pone.0138228.

Zhang, X.-d., Gao, X.-c., Li, Z.-w., Xu, L.-c., Li, Y.-b., Zhang, R.-h., Xue, J.-q., Guo, D.-w., 2020. The effect of amylose on kernel phenotypic characteristics, starch-related gene expression and amylose inheritance in naturally mutated high-amylose maize. J. Integr. Agric. 19, 1554–1564. https://doi.org/10.1016/S2095-3119(19)62779-6.

Zhuo, J., Wang, K., Wang, N., Xing, C., Peng, D., Wang, X., Qu, G., Kang, C., Ye, X., Li, Y., Yan, Y., Li, X., 2023. Pericarp starch metabolism is associated with caryopsis development and endosperm starch accumulation in common wheat. Plant Sci. 330, 111622 https://doi.org/10.1016/j.plantsci.2023.111622.